NANO LETTERS

Letter

pubs.acs.org/NanoLett

Noble Metal-Free Reduced Graphene Oxide-$Zn_xCd_{1-x}S$ Nanocomposite with Enhanced Solar Photocatalytic H_2-Production Performance

Jun Zhang,[†,‡] Jiaguo Yu,*[,†] Mietek Jaroniec,*[,§] and Jian Ru Gong*[,‡]

[†]State Key Laboratory of Advanced Technology for Materials Synthesis and Processing, College of Resource and Environmental Engineering, Wuhan University of Technology, Wuhan 430070, People's Republic of China

[‡]National Center for Nanoscience and Technology, 11 Zhongguancun Beiyitiao, Beijing 100190, People's Republic of China

[§]Department of Chemistry, Kent State University, Kent, Ohio 44242, United States

Supporting Information

ABSTRACT: Design and preparation of efficient artificial photosynthetic systems for harvesting solar energy by production of hydrogen from water splitting is of great importance from both theoretical and practical viewpoints. ZnS-based solid solutions have been fully proved to be an efficient visible-light driven photocatalysts, however, the H_2-production rate observed for these solid solutions is far from exciting and sometimes an expensive Pt cocatalyst is still needed in order to achieve higher quantum efficiency. Here, for the first time we report the high solar photocatalytic H_2-production activity over the noble metal-free reduced graphene oxide (RGO)-$Zn_xCd_{1-x}S$ nanocomposite prepared by a facile coprecipitation-hydrothermal reduction strategy. The optimized RGO-$Zn_{0.8}Cd_{0.2}S$ photocatalyst has a high H_2-production rate of 1824 μmol h^{-1} g^{-1} at the RGO content of 0.25 wt % and the apparent quantum efficiency of 23.4% at 420 nm (the energy conversion efficiency is ca. 0.36% at simulated one-sun (AM 1.5G) illumination). The results exhibit significantly improved photocatalytic hydrogen production by 450% compared with that of the pristine $Zn_{0.8}Cd_{0.2}S$, and are better than that of the optimized Pt-$Zn_{0.8}Cd_{0.2}S$ under the same reaction conditions, showing that the RGO-$Zn_{0.8}Cd_{0.2}S$ nanocomposite represents one of the most highly active metal sulfide photocatalyts in the absence of noble metal cocatalysts. This work creates a green and simple way for using RGO as a support to enhance the photocatalytic H_2-production activity of $Zn_xCd_{1-x}S$, and also demonstrates that RGO is a promising substitute for noble metals in photocatalytic H_2-production.

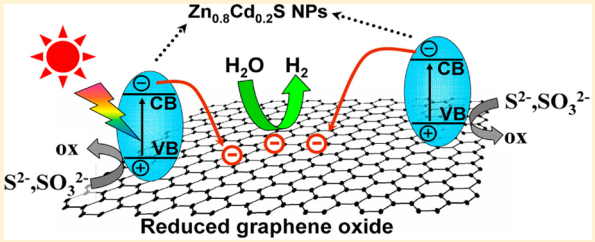

KEYWORDS: *Graphene, $Zn_xCd_{1-x}S$ solid solution, solar-light-driven, photocatalytic hydrogen production*

Since Honda and Fujishima discovered the photocatalytic splitting of water on TiO_2 electrodes in 1972,[1] this process attracted great attention because of its potential for hydrogen production, which is seen as a viable strategy for solving simultaneously the incoming energy and environmental problems.[2] So far, numerous active photocatalysts such as various oxide, sulfide, and oxynitride semiconductors have been developed for the aforementioned photocatalytic reaction.[3−7] Among them, metal sulfides and their composites are regarded as good candidates for photocatalytic H_2-production because of their suitable bandgap and catalytic function. Especially, ZnS is one of the most often applied photocatalysts due to its rapid generation of electron−hole pairs upon photoexcitation and highly negative reduction potentials of excited electrons.[8] Also, it shows the high activity for H_2 evolution under UV-light irradiation even without noble metal cocatalysts. Unfortunately, the bandgap of ZnS is 3.66 eV, which is too large to response under visible light.[9] Therefore, numerous attempts have been made on the development of doped ZnS and on the preparation of solid solutions (e.g., $Cd_xZn_{1-x}S$, Cu−$Zn_xCd_{1-x}S$, CuS−In_2S_3−ZnS) in order to shift the absorption edge of ZnS into the visible light range.[10−17] These ZnS-based solid solutions have been fully proved to be an efficient, low-toxic, and cost-effective visible-light driven photocatalysts for H_2-production from water splitting. However, the H_2-production rate observed for these solid solutions is far from exciting and sometimes an expensive Pt cocatalyst is still needed in order to achieve higher quantum efficiency.

Graphene, which offers an excellent electron transport property and possesses an extremely high specific surface area,[18] is highly desirable for use as a two-dimensional catalyst support.[19−24] Recently, some attempts have been made to combine graphene with semiconductor photocatalysts to enhance the photocatalytic H_2-production performance.[25−31] For instance, several visible-light-driven photocatalysts (such as CdS, $BiVO_4$, g-C_3N_4, $Sr_2Ta_2O_{7-x}N_x$) achieved increased photocatalytic water splitting activity by combining with graphene.[26−30] Nevertheless, in most cases the H_2-production

Received: May 16, 2012
Revised: August 9, 2012
Published: August 15, 2012

efficiencies of the graphene-based composites were still lower than that of semiconductors containing the Pt cocatalyst under the same conditions.[25−31] Here, for the first time we report the high photocatalytic H_2-production activity over the noble metal-free reduced graphene oxide (RGO)-$Zn_xCd_{1-x}S$ nanocomposite photocatalyst under simulated solar irradiation. The results exhibit significantly improved photocatalytic hydrogen production by 450% compared with that of the pristine $Zn_{0.8}Cd_{0.2}S$, and are better than that of the optimized Pt-$Zn_{0.8}Cd_{0.2}S$ under the same reaction conditions. Furthermore, the apparent quantum efficiency (QE) of 23.4% at 420 nm was obtained for the optimized RGO-$Zn_{0.8}Cd_{0.2}S$. To the best of our knowledge, the RGO-$Zn_{0.8}Cd_{0.2}S$ sample has higher QE than the graphene-based photocatalysts reported so far,[26,30] representing one of the most highly active metal sulfide photocatalysts in the absence of noble metal cocatalysts.[3−5]

It is well-known that the photocatalytic activity of $Zn_xCd_{1-x}S$ can be altered by varying the Cd/Zn ratio. The preliminary experiment (see Figure S1 in Supporting Information) shows that the prepared $Zn_xCd_{1-x}S$ solid solution without RGO exhibits the highest solar H_2-production rate at x = 0.8. Thus $Zn_{0.8}Cd_{0.2}S$ solid solution was used in the following study. The RGO-$Zn_{0.8}Cd_{0.2}S$ nanocomposites were prepared by a simple and environmental friendly coprecipitation-hydrothermal strategy[32] using $Cd(Ac)_2{\cdot}2H_2O$, $Zn(Ac)_2{\cdot}2H_2O$, and Na_2S as precursors in the presence of GO (see details in Supporting Information). During this process GO was reduced to RGO (see XPS, FT-IR, and Raman analysis in Supporting Information Figure S2) and $Zn_{0.8}Cd_{0.2}S$ nanoparticles were simultaneously formed on the RGO sheets. The weight ratios of GO to $Zn_{0.8}Cd_{0.2}S$ were 0, 0.1, 0.25, 0.5, 1, 2, and 5%, and the corresponding samples were labeled as GS0, GS0.1, GS0.25, GS0.5, GS1, GS2, and GS5, respectively. The energy dispersive X-ray (EDX) spectrum of sample GS0.25 shown in Supporting Information Figure S3 confirms the presence of S, Zn, and Cd elements. Figure 1a shows the typical TEM image of sample

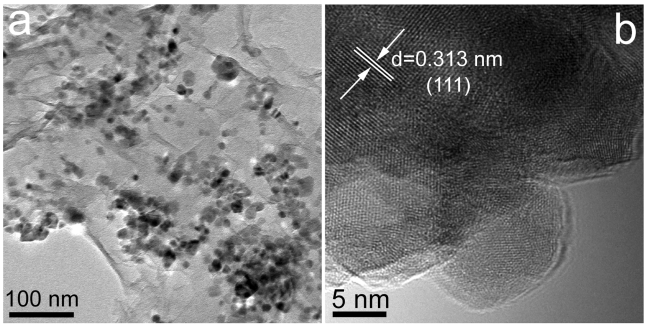

Figure 1. TEM (a) and HRTEM (b) images of sample GS0.25.

GS0.25 with $Zn_{0.8}Cd_{0.2}S$ nanoparticles well dispersed on the RGO nanosheets. The HRTEM image of GS0.25 (Figure 1b) clearly shows the lattice fringes, suggesting the well-defined crystal structure. The lattice spacing is about 0.313 nm, which can be assigned to the (111) plane of $Zn_{0.8}Cd_{0.2}S$. While, in comparison to the pure cubic ZnS (0.312 nm), the observed value of the (111) plane of $Zn_{0.8}Cd_{0.2}S$ is a little bit greater due to the larger radius of Cd^{2+} than that of Zn^{2+},[10] which is in agreement with the XRD results (Supporting Information Figure S4). The XRD peaks of all RGO-$Zn_{0.8}Cd_{0.2}S$ samples exhibit an obvious left-shift compared to the standard sphalerite ZnS [JCPDS No. 05-0566] due to the formation of $Zn_{0.8}Cd_{0.2}S$ solid solution. The peak position and intensity of these RGO-$Zn_{0.8}Cd_{0.2}S$ samples do not change much with increasing the RGO amount, implying that RGO does not have a significant influence on the phase structure and crystallinity of $Zn_{0.8}Cd_{0.2}S$ solid solutions. No characteristic diffraction peaks for RGO can be observed on these patterns because of the low amount and relatively low diffraction intensity.[26]

A comparison of the UV−vis diffuse reflectance spectra of the RGO-$Zn_{0.8}Cd_{0.2}S$ samples is depicted in Supporting Information Figure S5. For all the samples studied, a significant increase in the absorption at wavelengths shorter than 470 nm can be assigned to the intrinsic bandgap of $Zn_{0.8}Cd_{0.2}S$ solid solution. The bandgap energy (~2.53 eV) of the pure $Zn_{0.8}Cd_{0.2}S$ solid solution was estimated by extrapolating the straight portion of the $(ahv)^2$ versus photon energy (hv) curve to a = 0 according to the Kubelka−Munk function,[33,34] as illustrated in the inset of Supporting Information Figure S5. In addition, a broad background absorption in the visible-light region (500−800 nm) for the RGO-$Zn_{0.8}Cd_{0.2}S$ nanocomposite samples can be observed, and such absorption gradually increases by increasing the RGO content. The corresponding color of the nanocomposite samples becomes darker, that is, from light yellow to dark green. This is attributed to the presence of RGO in the RGO-$Zn_{0.8}Cd_{0.2}S$, which reduces reflection of light and thus enhances the absorption.[26,27] Further observation indicates that all the RGO-$Zn_{0.8}Cd_{0.2}S$ samples show almost the same absorption edge as that of the pure $Zn_{0.8}Cd_{0.2}S$ solid solution, implying RGO is not incorporated into the lattice of $Zn_{0.8}Cd_{0.2}S$.

Heterogeneous photocatalysis is a surface-based process, and a large surface area provides more surface active sites for the adsorption of reactant molecules, making the photocatalytic process more efficient.[35,36] Supporting Information Figure S6 shows the typical nitrogen adsorption−desorption isotherms and the corresponding pore size distribution curves of the GS0 and GS0.25 samples. The nitrogen adsorption−desorption isotherms are of type IV (Brunauer−Deming−Deming−Teller classification), indicating the presence of mesopores (2−50 nm). In addition, the isotherms show high adsorption at high relative pressures (P/P_0) (approaching 1.0), suggesting the formation of large mesopores and macropores.[37] The pore-size distributions (inset in Supporting Information Figure S6) of the samples indicate a wide pore-size distribution from 2 to 100 nm, further confirming the presence of mesopores and macropores. Supporting Information Table S1 displays all RGO-$Zn_{0.8}Cd_{0.2}S$ nanocomposites have larger Brunauer−Emmett−Teller (BET) surface areas than that of pure $Zn_{0.8}Cd_{0.2}S$ due to the presence of RGO with the extremely high surface area.

Figure 2 shows the photocatalytic H_2-production activity of the pristine $Zn_{0.8}Cd_{0.2}S$ solid solution and RGO-$Zn_{0.8}Cd_{0.2}S$ nanocomposites from an aqueous solution containing 0.35 M Na_2S and 0.25 M Na_2SO_3 under simulated solar irradiation (AM1.5, 100 mW/cm^2), together with that of Pt-GS0 and pure RGO for the purpose of comparison. As seen in Figure 2, $Zn_{0.8}Cd_{0.2}S$ solid solution without RGO shows some photocatalytic H_2-production activity, but the rate of H_2 evolution is low (403 μmol h^{-1} g^{-1}). The activity of the GS0.1 sample is remarkably enhanced in the presence of a small amount of RGO. The rate of H_2 evolution over RGO-$Zn_{0.8}Cd_{0.2}S$ increases with increasing RGO content, achieving a maximum of 1824 μmol h^{-1} g^{-1} at the RGO content of 0.25 wt %. The corresponding QE of 23.4% at 420 nm is higher than those of

dx.doi.org/10.1021/nl301831h | Nano Lett. 2012, 12, 4584−4589

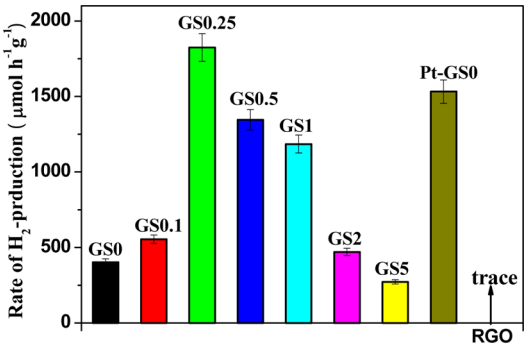

Figure 2. Comparison of the photocatalytic H_2-production activity under simulated solar irradiation over GS0, GS0.1, GS0.25, GS0.5, GS1, GS2, GS5, Pt-GS0, and RGO samples. Pt-GS0: GS0 loaded with the optimized 1 wt % of Pt cocatalyst.

the graphene-based photocatalysts reported so far,[26,30] showing that the RGO-$Zn_{0.8}Cd_{0.2}S$ sample represents one of the most highly active metal sulfide photocatalyts in the absence of noble metal cocatalysts.[3−5] A further increase in the content of RGO leads to a reduction in the photocatalytic activity. It is clearly visible in the case of GS5, the activity for H_2-production decreases dramatically and even below that of the pure $Zn_{0.8}Cd_{0.2}S$ solid solution. This is probably due to the following factors: (i) introduction of a large percentage of black RGO leads to shielding the incident light, thus preventing the generation of electrons from the inside of the $Zn_{0.8}Cd_{0.2}S$ nanoparticles;[38,39] (ii) excessive amount of RGO may cover the active sites on the surface of $Zn_{0.8}Cd_{0.2}S$ and also could hinder the contact of the sacrificial agents with $Zn_{0.8}Cd_{0.2}S$.[26] Therefore, a suitable content of RGO is crucial for optimizing the photocatalytic activity of composite photocatalysts, which can also be proved by the previous studies.[26,27,30] It should be noted that no hydrogen was detected when RGO alone was used as a photocatalyst, suggesting that the bare RGO is unlikely active for photocatalytic H_2 production under our experimental conditions. In addition, control experiments indicate that no appreciable hydrogen production was detected in the absence of either irradiation or photocatalyst, suggesting that hydrogen was produced by photocatalytic reaction.

It has been fully demonstrated that noble metals, especially Pt, can function as an efficient H_2-production promoter for many photocatalysts. Under solar irradiation, the $Zn_{0.8}Cd_{0.2}S$ solid solution loaded with the optimal 1 wt % Pt as cocatalyst significantly enhances the H_2-production activity up to 3.8 times that of pristine $Zn_{0.8}Cd_{0.2}S$ as shown in Supporting Information Figure S7. However, the activity of Pt−$Zn_{0.8}Cd_{0.2}S$ is still lower than that of the RGO-$Zn_{0.8}Cd_{0.2}S$ photocatalyst (GS0.25). In addition, as a carbon material, graphene is cheaper and more abundant than noble metals. Thus, it is fascinating to use RGO as a new cocatalyst for replacing noble metals in hydrogen production from water splitting.

Although there are numerous reports about powdered photocatalysts for H_2-production under visible light irradiation, only a few reports indicate solar energy conversion efficiencies especially for metal sulfide powdered photocatalysts.[13,16,17] Kudo et al. reported the H_2 gas evolved at a rate of 3.3 and 7.9 L m^{-2} h^{-1} for the samples of Pt-loaded $(AgIn)_{0.22}Zn_{1.56}S_2$ and Ru-loaded $Cu_{0.25}Ag_{0.25}In_{0.5}ZnS_2$ under one-sun (AM 1.5G) illumination,[13,17] and the solar energy conversion efficiencies was calculated to be ca. 0.85 and 2.0%, respectively. In addition, Ikeda et al. reported the H_2 evolution rate of more than 13.3 μmol h^{-1} on the sample of Ru-loaded $((Cu_xAg_{1-x})_2ZnSnS_4)_{0.9}(ZnS)_{0.4}$ under simulated solar irradiation (AM 1.5G).[16] In our work, the solar energy conversion efficiency of GS0.25 was determined to be 0.36%, which is lower than that of Pt-loaded $(AgIn)_{0.22}Zn_{1.56}S_2$ and Ru-loaded $Cu_{0.25}Ag_{0.25}In_{0.5}ZnS_2$, but higher than that of Ru-loaded $((Cu_xAg_{1-x})_2ZnSnS_4)_{0.9}(ZnS)_{0.4}$. Also, it should be noted that no expensive metals such as Pt, Ru, Ag as well as In were used in our RGO-$Zn_xCd_{1-x}S$ system.

Metal sulfides are usually not stable during the photocatalytic reaction and subjected to photocorrosion.[40,41] In our experiment, the stability of the RGO-$Zn_{0.8}Cd_{0.2}S$ (GS0.25) and pure $Zn_{0.8}Cd0.2S$ (GS0) were evaluated by performing the recycle experiments under the same conditions (see Supporting Information Figure S8). After four recycles, the photocatalytic H_2-production rate of sample GS0 decreases gradually, however sample GS0.25 does not exhibit any loss of activity, indicating the better stability of this nanocomposite for hydrogen generation. The high stability of the RGO-$Zn_{0.8}Cd_{0.2}S$ photocatalyst is attributed to the close interaction between RGO and $Zn_{0.8}Cd_{0.2}S$ solid solution,[42,43] which favors the vectorial transfer of the photogenerated electrons from the conduction band (CB) of $Zn_{0.8}Cd_{0.2}S$ to RGO. This space separation of the photogenerated electrons and holes is beneficial for preventing the reduction of Cd^{2+} and Zn^{2+}. Furthermore, high Na_2S concentration in the solution can suppress the oxidation of S^{2-} on $Zn_{0.8}Cd_{0.2}S$ (see further discussion in Supporting Information).

The high H_2-production activity of GS0.25 sample under solar irradiation can be explained from the scheme of Figure 3. Under solar irradiation, electrons are excited from the valence band (VB) populated by S 3p to the formed CB by hybridizing Zn 4s4p with Cd 5s5p,[44] which creates holes in VB. Normally, these charge carriers recombine rapidly resulting in a low photocatalytic H_2-production rate of $Zn_{0.8}Cd_{0.2}S$ itself. However, when $Zn_{0.8}Cd_{0.2}S$ nanoparticles are immobilized on

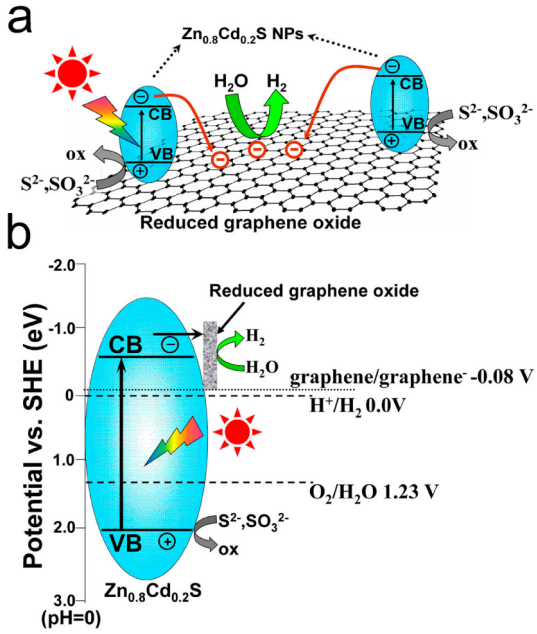

Figure 3. (a) Schematic illustration for the charge transfer and separation in the RGO-$Zn_{0.8}Cd_{0.2}S$ system; (b) proposed mechanism for photocatalytic H_2-production under simulated solar irradiation.

dx.doi.org/10.1021/nl301831h | Nano Lett. 2012, 12, 4584−4589

the surface of RGO, those photogenerated electrons in CB of $Zn_{0.8}Cd_{0.2}S$ tend to transfer to RGO, leading to the hole−electron separation. RGO can function as an electron collector and transporter to lengthen the lifetime of the charge carriers, consequently improving the charge separation and photocatalytic activity.[25−30] In addition, the unique features of RGO facilitate the photocatalytic reaction to take place not only on the surface of semiconductor catalysts, but also on the RGO sheet, greatly enlarging the reaction space.[26] Furthermore, since the potential of graphene/graphene$^{\bullet-}$ is about −0.08 V (vs SHE, pH = 0) as illustrated in Figure 3b,[45,46] it can act as a cocatalyst to promote the separation and transfer of photogenerated electrons from CB of $Zn_{0.8}Cd_{0.2}S$ to the RGO, where H^+ is reduced to hydrogen molecule ($E^0_{H+/H2}$ = 0 vs SHE, pH = 0); meanwhile, the holes in VB of $Zn_{0.8}Cd_{0.2}S$ can be consumed by the sacrificial agents (S^{2-}, SO_3^{2-}).

X-ray photoelectron spectroscopy (XPS) characterization of sample GS0.25 was carried out to examine the change in chemical status of Zn and Cd elements before and after photocatalytic reaction for 2 h. As shown in Supporting Information Figure S9a, the binding energies of 1021.7 and 1044.9 eV match well those of Zn $2p_{3/2}$ and $2p_{1/2}$ XPS peaks of Zn^{2+} in ZnS. The two peaks recorded in the Cd region at 404.9 and 411.6 eV (Supporting Information Figure S9b) are in agreement with the literature data for Cd^{2+} in CdS.[47] In addition, due to the formation of the solid solution, the XPS peaks of Zn and Cd exhibit a slight shift compared to that of the pure phase.[48] It should be noted after the 2 h photocatalytic reaction, the XPS peak positions of Zn 2p and Cd 3d all exhibit a slight right shift; especially for Cd 3d, the right shift is expected. This can be further concluded that under the solar irradiation the electrons are excited from VB to CB of $Zn_{0.8}Cd_{0.2}S$ and then transfer out from CB of $Zn_{0.8}Cd_{0.2}S$ into RGO and thus greatly enhances the separation of charge carriers and photocatalytic H_2-production performance.

To provide an additional evidence for the above suggested photocatalytic mechanism, the transient photocurrent responses of $Zn_{0.8}Cd_{0.2}S$ (GS0), RGO-$Zn_{0.8}Cd_{0.2}S$ (GS0.25), and Pt-GS0 (GS0 loaded with optimized 1 wt % of Pt cocatalyst) electrodes were recorded for several on−off cycles of solar irradiation. Figure 4 shows a comparison of the photocurrent−time (I−t) curves for the above three samples with typical on−off cycles of intermittent solar irradiation at a bias potential of 0.4 V. As seen from the figure, an apparently boosted photocurrent response appears for all three samples under solar illumination, and the on−off cycles of the photocurrent are reproducible. This indicates that most of photogenerated electrons are transported to the back contact across the sample to produce photocurrent under solar irradiation.[49] Notably, for the GS0 sample, the photocurrent curve has an obvious anodic photocurrent spike at the initial time of irradiation (see details in Supporting Information Figure S10). After the spike current has been attained, a continuous decrease in the photocurrent with time can be observed until reaching a constant current. Such photocurrent decay indicates that the recombination process occurs.[50] During the decay process, the holes accumulated at the $Zn_{0.8}Cd_{0.2}S$ surface competitively recombine with electrons from the CB of $Zn_{0.8}Cd_{0.2}S$ instead of being trapped or captured by reduced species in the electrolyte. In contrast, the anodic photocurrent spikes are not visible and the transient photocurrent shows a relatively slow response when the light is switched on and off for the Pt-GS0 and GS0.25 samples as shown respectively in panels b and c of Figure 4. The electrons trapped on the Pt nanoparticles and RGO in the composites are responsible for their slow photocurrent responses. It is not difficult to understand because Pt and graphene have lower Fermi level than that of the conduction band electrons and the trapping of conduction band electrons is a very rapid event.[51] Therefore, upon irradiation the traps in graphene are gradually filled with electrons, and then the trapped electrons further move to the deep traps. During this time, only a part of photoelectrons can transport to the back contact electrode until the deep traps are filled, which causes a slowly increased photocurrent response. Similarly, the slow response of the photocurrent decaying to zero by switching off the irradiation is controlled by charge carriers released from the traps.[51] It suggests that RGO (or Pt nanoparticles) can separate and store the photogenerated electrons, consequently reducing the recombination rate of the photogenerated electrons and holes and enhancing the production of photocurrent. Therefore, it is not surprising that the GS0 sample exhibits relative weak photocurrent because of the high recombination rate of electrons and holes.

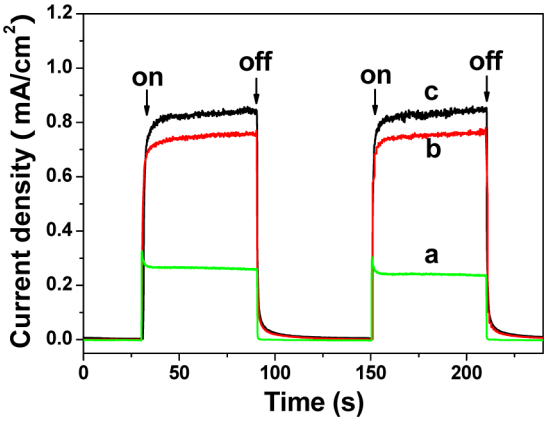

Figure 4. Transient photocurrent responses of the GS0 (a), GS0 loaded with 1 wt % Pt (b), and GS0.25 (c) samples in 0.1 M Na_2S + 0.02 M Na_2SO_3 mixed aqueous solution under solar irradiation.

In addition, the highest transient photocurrent was obtained for the GS0.25 sample. It is because graphene is an excellent electron-acceptor with superior conductivity due to its two-dimensional π-conjugation structure;[52] in the RGO-$Zn_{0.8}Cd_{0.2}S$ system, the excited electrons of $Zn_{0.8}Cd_{0.2}S$ can transfer from the CB of $Zn_{0.8}Cd_{0.2}S$ to RGO. Thus, in the GS0.25 sample RGO serves as an electron collector and tranporter which effectively suppresses the charge recombination, leaving more charge carriers to form reactive species which in turn results in the highest photocurrent response and photocatalytic H_2-production rate. The comparison of the I−V characteristics for the three samples in Supporting Information Figure S11 also proves the highest photocurrent in the GS0.25 sample, which further confirms that the introduction of RGO can promote the separation of electrons and holes and thus photocatalytic activities.

Electrochemical impedance spectra (EIS) analysis has become a powerful tool in studying the charge transfer process occurring in the three-electrode system and the EIS Nynquist plots of the three samples are shown in Figure 5. The high-frequency response is due to the charge transfer (or electrochemical reaction) at the Pt counter electrode, while

dx.doi.org/10.1021/nl301831h | Nano Lett. 2012, 12, 4584−4589

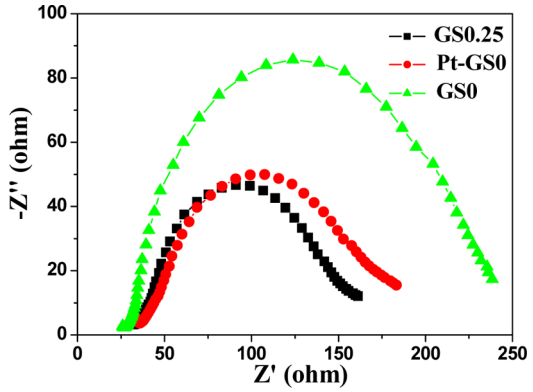

Figure 5. Nyquist plots of GS0, GS0 loaded with 1 wt % Pt, and GS0.25 electrodes in 0.1 M Na_2S + 0.02 M Na_2SO_3 aqueous solution under solar irradiation.

the intermediate-frequency response is associated with the electron transport and transfer at the $Zn_{0.8}Cd_{0.2}S$/electrode interface.[53,54] The RGO-$Zn_{0.8}Cd_{0.2}S$ sample (GS0.25) shows the smallest semicircle in the middle-frequency region in comparison to the pristine $Zn_{0.8}Cd_{0.2}S$ (GS0) and GS0 loaded with 1 wt % Pt (Pt-GS0) electrodes, which indicates the fastest interfacial electron transfer.[26,53] That is, because of the excellent conductivity, the introduction of RGO can benefit the charge transfer in the RGO-$Zn_{0.8}Cd_{0.2}S$ system and thus lower the charge recombination. Overall, RGO can function as an electron collector and transporter in the composite and inhibit the charge recombination and thus significantly enhance the photocatalytic H_2-production activity.

In summary, the high photocatalytic H_2-production performance under simulated solar irradiation over the RGO-$Zn_{0.8}Cd_{0.2}S$ photocatalyst using a feasible coprecipitation-hydrothermal reduction strategy was reported for the first time. The as-prepared RGO-$Zn_{0.8}Cd_{0.2}S$ sample reached a high H_2-production rate of 1824 μmol h^{-1} g^{-1} at the RGO content of 0.25 wt % and the QE of 23.4% at 420 nm, which has higher QE than the graphene-based photocatalysts reported so far. The energy conversion efficiency is found to be ca. 0.36% at one-sun (AM 1.5G) illumination. Compared with the pristine $Zn_{0.8}Cd_{0.2}S$, the RGO-$Zn_{0.8}Cd_{0.2}S$ sample showed a significantly enhanced hydrogen production performance by a factor of 4.5 and even higher than that of the optimized Pt–$Zn_{0.8}Cd_{0.2}S$ sample under the same reaction conditions. The results demonstrate that the unique features of RGO make it an excellent supporting material for $Zn_{0.8}Cd_{0.2}S$ nanoparticles as well as a good electron collector and transporter. Our work shows a green and simple way of using RGO as a support for enhancing H_2-production photoactivity of $Zn_{0.8}Cd_{0.2}S$ nanoparticles and also demonstrates that RGO is a promising substitute for noble metals in photocatalytic H_2-production.

■ ASSOCIATED CONTENT

Supporting Information

Additional information about sample preparation, characterization and physicochemical properties, measurements of photocatalytic H_2-prodution activity, EDX, FT-IR, Raman, UV–vis, XRD, XPS, and photoelectrochemical performance. This material is available free of charge via the Internet at http://pubs.acs.org.

■ AUTHOR INFORMATION

Corresponding Author

*E-mail: (J.Y.) jiaguoyu@yahoo.com; (M.J.) jaroniec@kent.edu; (J.R.G.) gongjr@nanoctr.cn.

Notes

The authors declare no competing financial interest.

■ ACKNOWLEDGMENTS

This work was partially supported by the National Natural Science Foundation of China (Nos. 51102190, 20877061, 51072154, 21005023, and 91123003) and the Natural Science Foundation of Hubei Province (No. 2010CDA078). Also, this work was financially supported by the National Basic Research Program of China (Nos. 2009CB939704, 2011CB933401, and 2012CB934000) and Self-determined and Innovative Research Funds of SKLWUT.

■ REFERENCES

(1) Fujishima, A.; Honda, K. *Nature* **1972**, *238*, 37–38.
(2) Xiang, Q. J.; Yu, J. G.; Wang, W. G.; Jaroniec, M. *Chem. Commun.* **2011**, *47*, 6906–6908.
(3) Kudo, A.; Miseki, Y. *Chem. Soc. Rev.* **2009**, *38*, 253–278.
(4) Navarro, R. M.; Alvarez-Galvan, M. C.; de la Mano, J. A. V.; Al-Zahrani, S. M.; Fierro, J. L. G. *Energy Environ. Sci.* **2010**, *3*, 1865–1882.
(5) Johnson, T. C.; Morris, D. J.; Wills, M. *Chem. Soc. Rev.* **2010**, *39*, 81–88.
(6) Ran, J. R.; Yu, J. G.; Jaroniec, M. *Green Chem.* **2011**, *13*, 2708–2713.
(7) Qi, L. F.; Yu, J. G.; Jaroniec, M. *Phys. Chem. Chem. Phys.* **2011**, *13*, 8915–8923.
(8) Zhang, J.; Yu, J. G.; Zhang, Y. M.; Li, Q.; Gong, J. R. *Nano Lett.* **2011**, *11*, 4774–4779.
(9) Reber, J. F.; Meier, K. *J. Phys. Chem.* **1984**, *88*, 5903–5913.
(10) Wang, L.; Wang, W. Z.; Shang, M.; Yin, W. Z.; Sun, S. M.; Zhang, L. *Int. J. Hydrogen Energy* **2010**, *35*, 19–25.
(11) Zhang, J.; Liu, S. W.; Yu, J. G.; Jaroniec, M. *J. Mater. Chem.* **2011**, *21*, 14655–14662.
(12) Yu, J. G.; Zhang, J.; Jaroniec, M. *Green Chem.* **2010**, *12*, 1611–1614.
(13) Tsuji, I.; Kato, H.; Kudo, A. *Chem. Mater.* **2006**, *18*, 1969–1975.
(14) Shen, S. H.; Zhao, L.; Zhou, Z. H.; Guo, L. J. *J. Phys. Chem. C* **2008**, *112*, 16148–16155.
(15) Li, Y. X.; Chen, G.; Wang, Q.; Wang, X.; Zhou, A. K.; Shen, Z. Y. *Adv. Funct. Mater.* **2010**, *20*, 3390–3398.
(16) Ikeda, S.; Nakamura, T.; Harada, T.; Matsumura, M. *Phys. Chem. Chem. Phys.* **2010**, *42*, 13943–13949.
(17) Tsuji, I.; Kato, H.; Kobayashi, H.; Kudo, A. *J. Am. Chem. Soc.* **2004**, *126*, 13406–13413.
(18) Allen, M. J.; Tung, V. C.; Kaner, R. B. *Chem. Rev.* **2010**, *110*, 132–145.
(19) Lightcap, I. V.; Kosel, T. H.; Kamat, P. V. *Nano Lett.* **2010**, *10*, 577–583.
(20) Xiang, Q. J.; Yu, J. G.; Jaroniec, M. *Chem. Soc. Rev.* **2012**, *41*, 782–796.
(21) Eda, G.; Fanchini, G.; Chhowalla, M. *Nat. Nanotechnol.* **2008**, *3*, 270–274.
(22) Zeng, P.; Zhang, Q. G.; Peng, T. Y.; Zhang, X. H. *Phys. Chem. Chem. Phys.* **2011**, *13*, 21496–21502.
(23) Zhang, N.; Zhang, Y. H.; Pan, X. Y.; Yang, M. Q.; Xu., Y. J. *J. Phys. Chem. C* **2012**, DOI: DOI: 10.1021/jp303503c.
(24) Yu, X. Y.; Chen, Z. H.; Kuang, D. B.; Su, C. Y. *ChemPhysChem.* **2012**, *13*, 2654–2658.
(25) Zhang, X. Y.; Li, H. P.; Cui, X. L.; Lin, Y. H. *J. Mater. Chem.* **2010**, *20*, 2801–2806.
(26) Li, Q.; Guo, B. D.; Yu, J. G.; Ran, J. R.; Zhang, B. H.; Yan, H. J.; Gong, J. R. *J. Am. Chem. Soc.* **2011**, *133*, 10878–10884.

(27) Jia, L.; Wang, D. H.; Huang, Y. X.; Xu, A. W.; Yu, H. Q. *J. Phys. Chem. C* **2011**, *115*, 11466−11473.
(28) Xiang, Q. J.; Yu, J. G.; Jaroniec, M. *J. Phys. Chem. C* **2011**, *115*, 7355−7363.
(29) Ng, Y. H.; Iwase, A.; Kudo, A.; Amal, R. *J. Phys. Chem. Lett.* **2010**, *1*, 2607−2612.
(30) Mukherji, A.; Seger, B.; Lu, G. Q.; Wang, L. Z. *ACS Nano* **2011**, *5*, 3483−3492.
(31) Lv, X. J.; Fu, W. F.; Chang, H. X.; Zhang, H.; Cheng, J. S.; Zhang, G. J.; Song, Y.; Hu, C. Y.; Li, J. H. *J. Mater. Chem.* **2012**, *22*, 1539−1546.
(32) Zhou, Y.; Bao, Q. L.; Tang, L. A. L.; Zhong, Y. L.; Loh, K. P. *Chem. Mater.* **2009**, *21*, 2950−2956.
(33) Zhou, M. H.; Yu, J. G. *J. Hazard. Mater.* **2008**, *152*, 1229−1236.
(34) Kubelka, P. *J. Opt. Soc. Am.* **1948**, *38*, 448−457.
(35) Yu, J. G.; Zhang, L. J.; Cheng, B.; Su, Y. R. *J. Phys. Chem. C* **2007**, *111*, 10582−10589.
(36) Yang, J.; Zhang, J.; Zhu, L. W.; Chen, S. Y.; Zhang, Y. M.; Tang, Y.; Zhu, Y. L.; Li, Y. W. *J. Hazard. Mater.* **2006**, *137*, 952−958.
(37) Sing, K. S. W.; Everett, D. H.; Haul, R. A. W.; Moscou, L.; Pierotti, R. A.; Rouquerol, J.; Siemieniewska, T. *Pure Appl. Chem.* **1985**, *57*, 603−619.
(38) Yu, J. G.; Ran, J. R. *Energy Environ. Sci.* **2011**, *4*, 1364−1371.
(39) Yu, J. G.; Hai, Y.; Cheng, B. *J. Phys. Chem. C* **2011**, *115*, 4953−4958.
(40) Frank, A. J.; Honda, K. *J. Phys. Chem.* **1982**, *86*, 1933−1935.
(41) Bao, N.; Shen, L.; Takata, T.; Domen, K.; Gupta, K.; Yanagisawa, A. *J. Phys. Chem. C* **2007**, *111*, 17527−17534.
(42) Zhou, F.; Shi, R.; Zhu, Y. F. *J. Mol. Catal.: A* **2011**, *340*, 77−82.
(43) Xu, T. G.; Zhang, L. W.; Cheng, H. Y.; Zhu, Y. F. *Appl. Catal., B* **2011**, *101*, 382−387.
(44) Liu, G. J.; Zhao, L.; Ma, L. J.; Guo, L. J. *Catal. Commun.* **2008**, *9*, 126−130.
(45) Zhou, K. F.; Zhu, Y. H.; Yang, X. L.; Jiang, X.; Li, C. Z. *New J. Chem.* **2011**, *35*, 353−359.
(46) Wang, X.; Zhi, L. J.; Mullen, K. *Nano Lett.* **2008**, *8*, 323−327.
(47) Moulder, J. F.; Stickle, W. F.; Sobol, P. E.; Bomben, K. D.; Chastain, J. *Handbook of X-ray Photoelectron Spectroscopy*; Physical Electronics, Inc.: Eden Prairie, MN, 1992.
(48) Deshpande, A.; Shah, P.; Gholap, R. S.; Gupta, N. M. *J. Colloid. Interface Sci.* **2009**, *333*, 263−268.
(49) Hagfeldt, A.; Lindstrom, H.; Sodergren, S.; Lindquist, S. *J. Electroanal. Chem.* **1995**, *381*, 39−46.
(50) Xu, Z. H.; Yu, J. G. *Nanoscale* **2011**, *3*, 3138−3144.
(51) Yu, J. G.; Dai, G. P.; Huang, B. B. *J. Phys. Chem. C* **2009**, *113*, 16394−16401.
(52) Novoselov, K. S.; Geim, A. K.; Morozov, S. V.; Jiang, D.; Zhang, Y.; Dubonos, S. V.; Grigorieva, I. V.; Firsov, A. A. *Science* **2004**, *306*, 666−669.
(53) Yu, J. G.; Fan, J. J.; Cheng, Bei. *J. Power Source* **2011**, *196*, 7891−7898.
(54) Jana, A.; Bhattacharya, C.; Datta, J. *Electrochim. Acta.* **2010**, *55*, 6553−6562.

Supporting Information

Noble Metal-Free Reduced Graphene Oxide-$Zn_xCd_{1-x}S$ Nanocomposite with Enhanced Solar Photocatalytic H_2-Production Performance

Jun Zhang,[†,‡] Jiaguo Yu,[†,*] Mietek Jaroniec,[§,*] Jian Ru Gong[‡,*]

[†] State Key Laboratory of Advanced Technology for Materials Synthesis and Processing, College of Resource and Environmental Engineering, Wuhan University of Technology, Wuhan 430070, People's Republic of China

[‡] National Center for Nanoscience and Technology, 11 Zhongguancun Beiyitiao, Beijing 100190, People's Republic of China

[§]Department of Chemistry, Kent State University, Kent, Ohio 44242, USA

*Correspondence: jiaguoyu@yahoo.com, jaroniec@kent.edu, gongjr@nanoctr.cn

Sample preparation. All the reagents were of analytical grade and were used without further purification. Distilled water was used in all experiments. Graphene oxide (GO) sheets were provided by Xiamen Knano Graphene Technology Corporation Limited, Xiamen, P.R. China. Since preliminary studies (see Figure S1) showed that the $Zn_xCd_{1-x}S$ solid solution with x = 0.8 without GO exhibited highest solar H_2-production, this composition was chosen in the current study. In a typical synthesis of the composite, 0.352 g of $Zn(Ac)_2\ 2H_2O$ and 0.123 g of $Cd(Ac)_2\ 2H_2O$ were dispersed in distilled water (30 mL), and then the specified volume of GO dispersed in a aqueous solution (0.5 g/L) was added. The weight ratios of GO to $Zn_{0.8}Cd_{0.2}S$ were 0, 0.1%, 0.25%, 0.5%, 1%, 2% and 5%, and the resulting samples were labeled as GS0, GS0.1, GS0.25, GS0.5, GS1, GS2 and GS5, respectively. The volume of the resulting solution was adjusted to 50 mL with deionized water and then 10 mL of 0.3 M Na_2S aqueous solution was added dropwise followed by stirring for

2 h at room temperature. After that, the suspension was transferred to a 100-mL teflon-lined autoclave and maintained at 160 ^{o}C for 4 h. The final products were respectively rinsed three times with distilled water and ethanol, and dried at 60 ^{o}C for 10 h. For comparison, Pt loaded-pure $Zn_{0.8}Cd_{0.2}S$ sample was also prepared by photoreduction method using H_2PtCl_6 solution as Pt source. The bare RGO sample without $Zn_{0.8}Cd_{0.2}S$ was prepared under the same experimental conditions.

Characterization. X-ray diffraction (XRD) patterns were obtained on an X-ray diffractometer (type HZG41B-PC) using Cu Kα radiation at a scan rate of 0.05^{o} 2θ s^{-1}. X-ray photoelectron spectroscopy (XPS) measurements were performed in an ultrahigh vacuum VG ESCALAB 210 electron spectrometer equipped with a multi-channel detector. The spectra were excited using Mg Kα (1253.6 eV) radiation (operated at 200 W) of a twin anode in the constant analyzer energy mode with a pass energy of 30 eV. All the binding energies were referenced to the C1s peak at 284.8 eV of the surface adventitious carbon. Scanning electron microscopy (SEM) was carried out by an S-4800 field emission SEM (FESEM, Hitachi, Japan). Transmission electron microscopy (TEM) analyses were conducted by a JEM-2010 electron microscope (JEOL, Japan) at an acceleration voltage of 200 kV. The Brunauer-Emmett-Teller (BET) specific surface area (S_{BET}) of the powders was analyzed by nitrogen adsorption using a Micromeritics ASAP 2020 nitrogen adsorption apparatus (USA). A desorption isotherm was used to determine the pore size distribution by the Barret-Joyner-Halender (BJH) method, assuming a cylindrical pore model. UV-vis diffused reflectance spectra of the samples studied were obtained for the dry-pressed disk samples using a UV-vis spectrotometer (UV2550, Shimadzu, Japan). $BaSO_4$ was used as a reflectance standard in a UV-vis diffuse reflectance experiment.

Photocatalytic hydrogen production. The photocatalytic hydrogen evolution experiments were performed in a 175 mL Pyrex flask at ambient temperature and atmospheric pressure, and openings of the flask were sealed with silicone rubber septum. The light was produced by a solar simulator (AM1.5, 100 mW/cm^2, Newport 91160) and the area of surface irradiated in the cylinder reactor was about 16.5 cm^2. In a typical photocatalytic experiment, 50 mg of catalyst was dispersed with a constant stirring in 80 mL of mixed aqueous solution containing 0.35 M Na_2S and 0.25 M Na_2SO_3. Before irradiation, the system was bubbled with nitrogen for 30 min to remove the air inside and to ensure that the reaction system is under anaerobic conditions. A 0.4 mL of gas was intermittently sampled through the septum, and hydrogen was analyzed by gas chromatograph (GC-14C,

Shimadzu, Japan, TCD, nitrogen as a carrier gas and 5Å molecular sieve column). All glassware was carefully rinsed with distilled water prior to use.

The apparent quantum efficiency (QE) was measured under the same photocatalytic reaction conditions. The light was produced by a solar simulator (AM1.5, 100 mW/cm^2, Newport 91160), and the intensity and number of photons of the light source at 420 nm were measured by a 420 nm band pass filter and an irradiate-meter. The QE was finally calculated according to Eq. (1):

$$\begin{aligned} \mathrm{QE}[\%] &= \frac{\text{number of reacted electrons}}{\text{number of incident photons}} \times 100 \\ &= \frac{\text{number of evolved } \mathrm{H_2} \text{ molecules} \times 2}{\text{number of incident photons}} \times 100 \end{aligned} \quad (1)$$

The energy conversion efficiency (η_c) under 1-sun (AM 1.5G) illumination was determined by Eq. (2)[1], where ΔG^0 (J mol^{-1}) is the standard Gibbs energy for the chemical reaction forming the hydrogen, R (mol s^{-1}) is the rate of generation of hydrogen in its standard state, E_s (W m^{-2}) is the incident solar irradiance and A (m^2) is the irradiated area.

$$\eta_c = \Delta G^0 R / E_s A \quad (2)$$

Photoelectrochemical measurements. The working electrodes were prepared as follows: 0.2 g of photocatalyst was grinded with 0.06 g polyethylene glycol (PEG, molecular weight: 20000) and 0.5 mL water to make a slurry. The slurry was then coated onto a 2 cm×1.2 cm F-doped SnO_2-coated glass (FTO glass) electrode by the doctor blade method. Next, the resulting electrodes were dried in an oven and calcined at 450 ^{o}C for 30 min in a N_2 gas flow. All electrodes studied had a similar film thickness (10~11 μm). Photocurrents were measured using an electrochemical analyzer (CHI660C Instruments) with a standard three-electrode system using the prepared samples as the working electrodes with an active area of ca. 1.44 cm^2, a Pt wire as the counter electrode, and Ag/AgCl (saturated KCl) as a reference electrode. The light was produced by a solar simulator (AM1.5, 100 mW/cm^2, Newport 91160), and 0.1 M Na_2S and 0.02 M Na_2SO_3 mixed aqueous solution was used as the electrolyte. The I-V characteristics were measured in the same three-electrode system and the bias sweep range was from -0.4 to 0.8 V with the step size of 5 mV. Electrochemical impedance spectra (EIS) measurements were also carried out in the above mentioned three-electrode system and recorded over a frequency range of 0.005-10^5 Hz with ac amplitude of 10 mV at 0.5 V.

Table S1. Effect of RGO content on the physical properties of the RGO-$Zn_{0.8}Cd_{0.2}S$ samples.

Sample	*RGO content (wt %)*	S_{BET} *(m^2/g)*	*Pore volume (cm^3/g)*	*Average pore size (nm)*
GS0	0	79	0.27	13.6
GS0.1	0.1	80	0.28	14.0
GS0.25	0.25	81	0.30	15.1
GS0.5	0.5	83	0.30	14.4
GS1	1	89	0.29	14.8
GS2	2	91	0.27	13.3
GS5	5	101	0.28	13.1

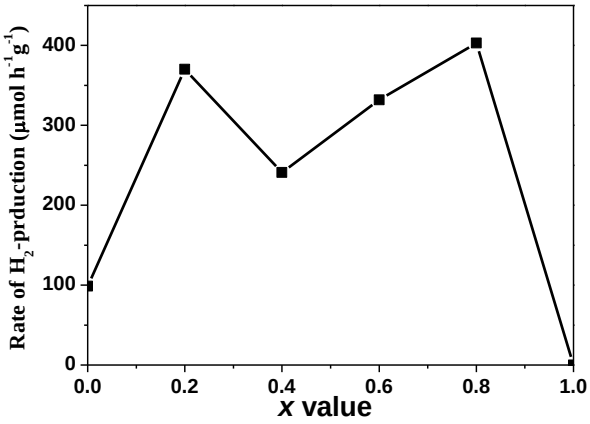

Figure S1. H_2-production activity under solar irradiation of $Zn_xCd_{1-x}S$ solid solutions with different x value.

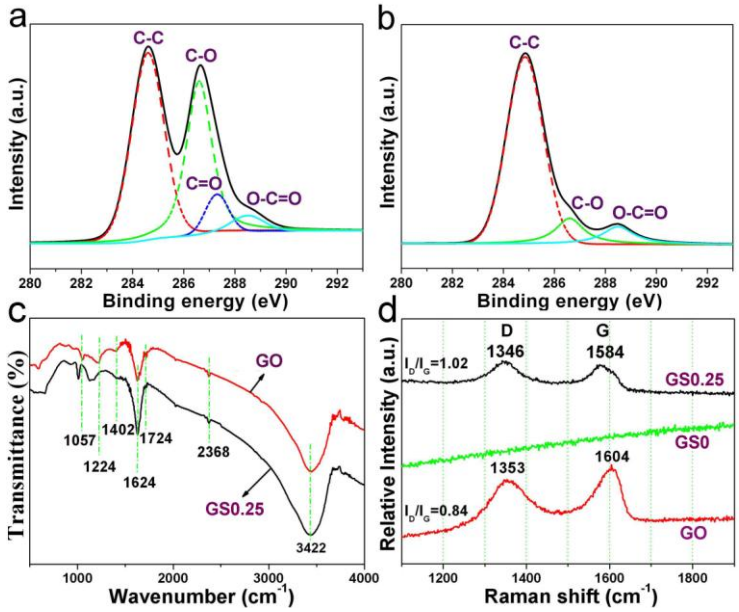

Figure S2. High-resolution XPS spectra of C 1s from: (a) GO and (b) GS0.25; (c) FT-IR spectra of GO and GS0.25; (d) Raman spectra of GO, GS0 and GS0.25 samples.

As shown in Figure S2a, the XPS spectrum of C1s from GO (solid black line) can be deconvoluted into four smaller peaks (dashed lines) which are ascribed to the following functional groups: sp^2 bonded carbon (C-C, 284.6 eV), epoxy/hydroxyls (C-O, 286.6 eV), carbonyls (C=O, 287.3 eV), and carboxyl (O-C=O, 288.5 eV).[2,3] In comparison to the GO spectrum, the peak for C=O in the GS0.25 (Figure S2b) almost vanishes, and the peaks for C-O and O-C=O (dashed lines) still exist but their intensities are much smaller. In addition, based on the XPS data, the oxygen content decreases from 29.1% in GO to 9.3% in GS0.25. These results indicate that about 70% of the oxygen-containing functional groups were removed during hydrothermal reduction process.

Figure S2c shows the FT-IR spectra of GO and GS0.25; the characteristic peaks of GO, including C-O stretching at 1057 cm^{-1}, C-OH stretching at 1224 cm^{-1}, carboxyl O-H deformation at 1402 cm^{-1}, skeletal vibration of unoxidized graphitic domains at 1624 cm^{-1} and C=O stretching at 1724 cm^{-1} were clearly observed in the spectrum recorded for GO.[4,5] The broad bands in the 3400-3800 cm^{-1} region and at 2368 cm^{-1} are related to physically adsorbed H_2O and CO_2 from the atmosphere, respectively. For the GS0.25 sample, the peaks reflecting functional groups in GO are much less intense or absent, especially those at 1224 cm^{-1}, 1402 cm^{-1} and 1724 cm^{-1} which are all assigned to the oxygen-containing groups. These results support that the substantial reduction of GO occurred, which is in a good agreement with the XPS analysis. Raman spectroscopy has been commonly used for characterization of graphitic

materials. Figure S2d shows the Raman spectra of GO, pure $Zn_{0.8}Cd_{0.2}S$ (sample GS0) and the RGO-$Zn_{0.8}Cd_{0.2}S$ (sample GS0.25). There are two characteristic peaks at about 1353 cm^{-1} (D band) and 1604 cm^{-1} (G band)[3] for the graphitized structures observed clearly for GO. For the RGO-$Zn_{0.8}Cd_{0.2}S$ sample (GS0.25) two typical bands at about 1346 and 1584 cm^{-1} are observed, confirming the presence of graphene in this composite. However, in comparison to GO, the D band moves to 1346 cm^{-1} and G band shifts to 1584 cm^{-1}, which matches the value of pristine graphite (1586 cm^{-1}), indicating the reduction of GO. As well, the RGO-$Zn_{0.8}Cd_{0.2}S$ shows an increased D/G intensity ratio compared to that of pure GO. This change suggests a decrease in the average size of the in-plane sp^2 domains upon reduction of the GO.[6] Based on the above results, it is reasonable to conclude that during co-precipitation-hydrothermal process in the presence of GO, $Zn(Ac)_2$, $Cd(Ac)_2$ and Na_2S, GO was *in situ* reduced and the RGO-$Zn_{0.8}Cd_{0.2}S$ nanocomposites were finally obtained.

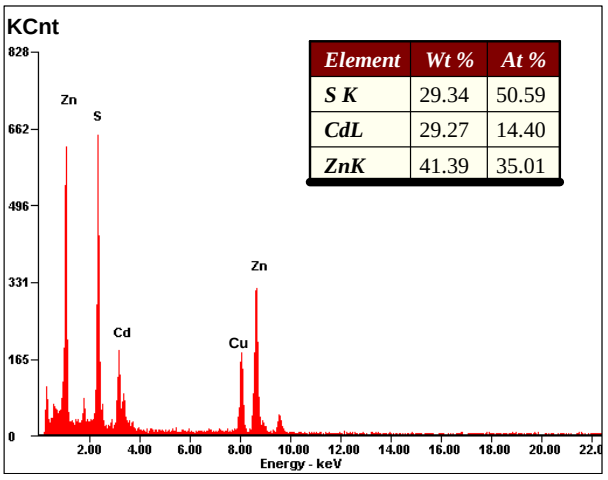

Element	Wt %	At %
S K	29.34	50.59
CdL	29.27	14.40
ZnK	41.39	35.01

Figure S3. The electron dispersive X-ray (EDX) spectrum for GS0.25 sample; this spectrum was recorded by using an Oxford Instruments X-ray analysis system. The Cu peak originates from the TEM copper grid used as a sample holder. The EDX spectrum confirms the presence of S, Zn and Cd elements, and the molar ratio of Zn to Cd is found to be ca. 0.72:0.28.

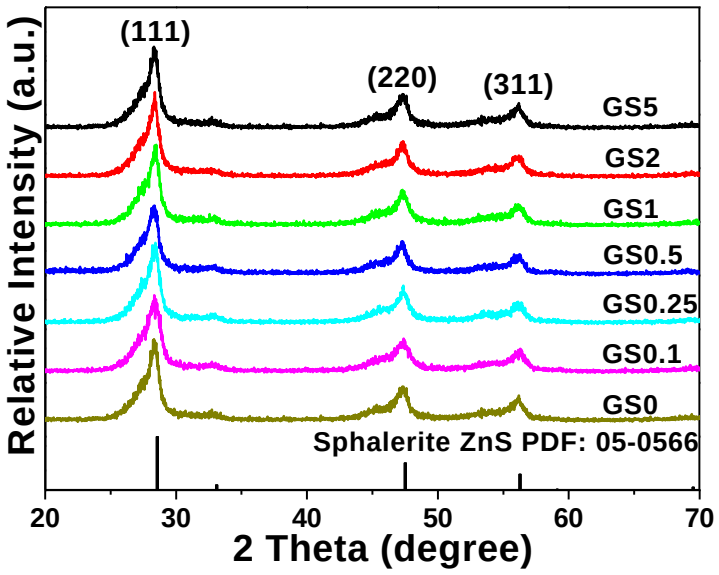

Figure S4. XRD patterns of the RGO-$Zn_{0.8}Cd_{0.2}S$ samples.

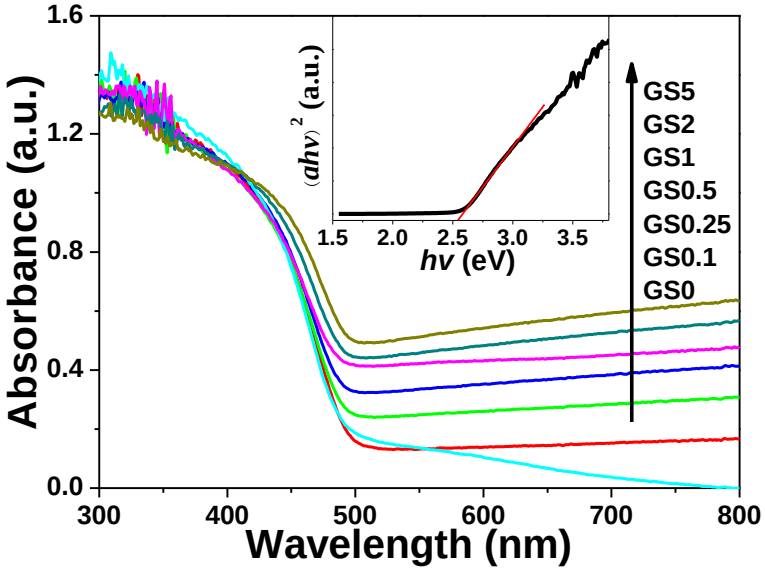

Figure S5. UV-vis diffuse reflectance spectra of the RGO-$Zn_{0.8}Cd_{0.2}S$ samples.

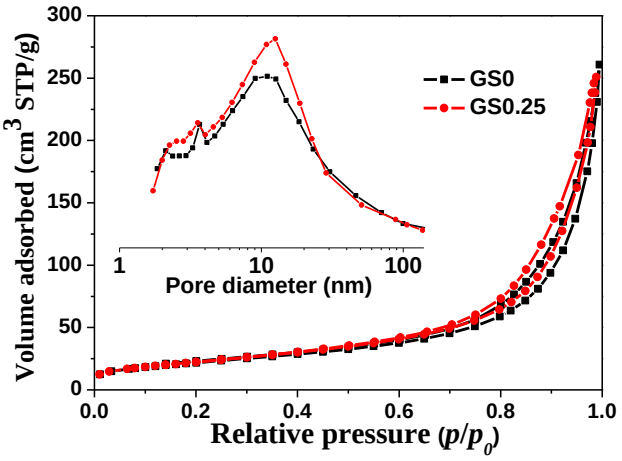

Figure S6. Nitrogen adsorption-desorption isotherms and the corresponding pore size distribution curves of the GS0 and GS0.25 samples.

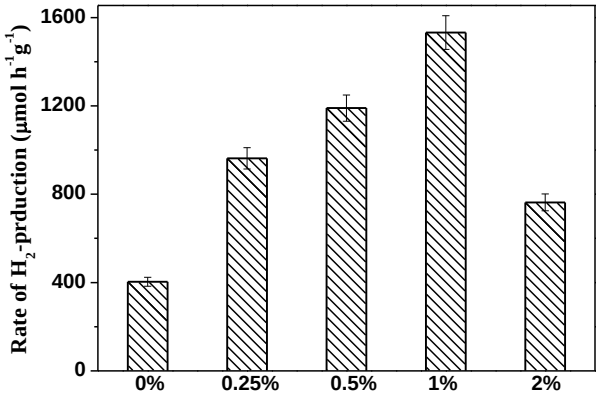

Figure S7. Comparison of the solar photocatalytic H_2-production activity of $Zn_{0.8}Cd_{0.2}S$ solid solution (sample GS0) with different Pt loading (wt %).

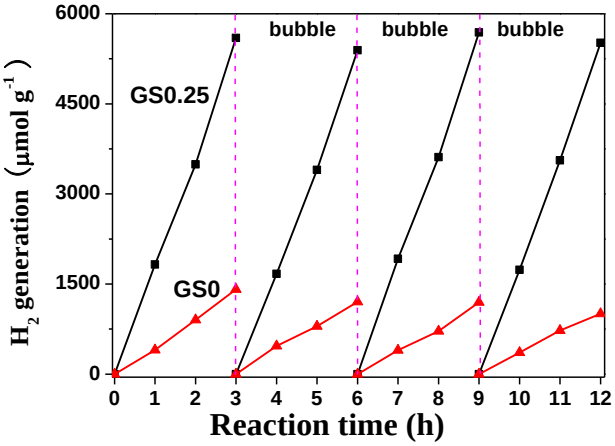

Figure S8. Time course of photocatalytic H_2-production over samples GS0.25 and GS0; every three hours the reaction system is bubbled with N_2 for 30 min to remove the H_2 inside.

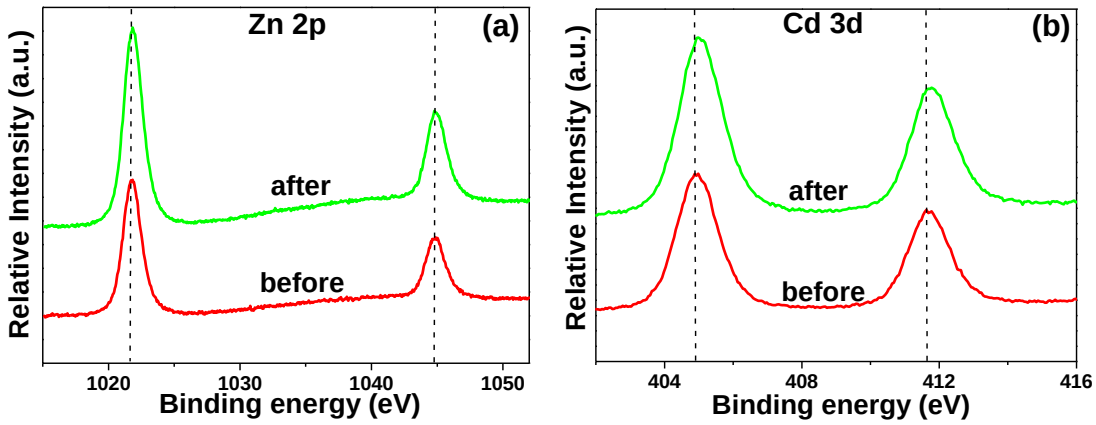

Figure S9. High-resolution XPS spectra of Zn 2p (a) and Cd 3d (b) for the GS0.25 sample before and after 2 h photocatalytic H_2-production under simulated solar irradiation.

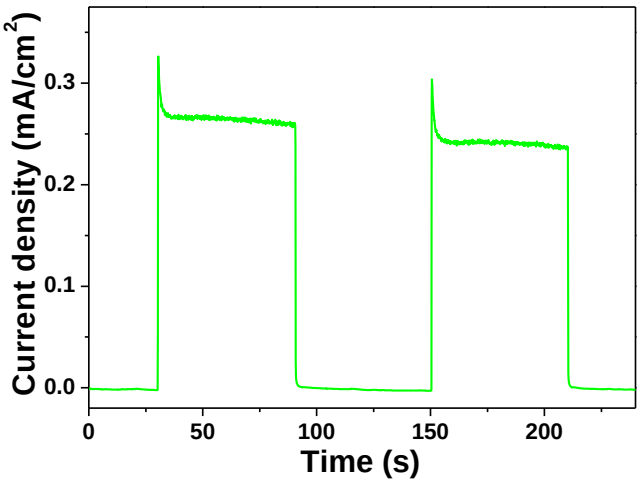

Figure S10. Individual transient photocurrent responses of sample GS0 in 0.1 M Na_2S + 0.02 M Na_2SO_3 aqueous solution under solar irradiation.

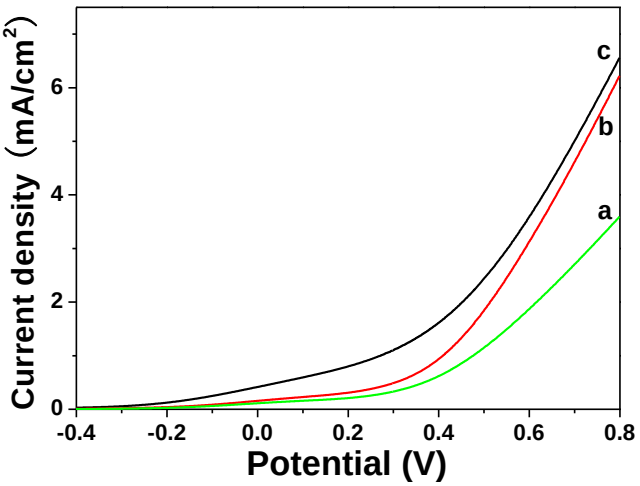

Figure S11. *I-V* characteristics of the GS0 (a), GS0 loaded with 1 wt% Pt (b), and GS0.25 (c) samples under solar irradiation.

During the illumination on the RGO-$Zn_{0.8}Cd_{0.2}S$ nanocomposite from an aqueous solution containing Na_2S and Na_2SO_3, hydrogen was evolved and due to the strong reduction capacity of S^{2-} ions, the photogenerated holes irreversibly oxidize the S^{2-} ions instead of water. Different reactions occurred for the whole procedure can be represented as follows:[7]

$$Zn_{0.8}Cd_{0.2}S + h\nu \longrightarrow h^+ + e^- \quad (1)$$

$$2e^- + 2H_2O \longrightarrow H_2 + 2OH^- \quad (2)$$

$$SO_3^{2-} + 2OH^- + 2h^+ \longrightarrow SO_4^{2-} + 2H^+ \quad (3)$$

$$2S^{2-} + 2h^+ \longrightarrow S_2^{2-} \quad (4)$$

$$S_2^{2-} + SO_3^{2-} \longrightarrow S_2O_3^{2-} + S^{2-} \quad (5)$$

REFERENCES

(1) Bolton, J. R. *Solar Energy* **1996**, *57*, 37-50.

(2) Murugan, A. V.; Muraliganth, T.; Manthiram, A. *Chem. Mater*. **2009**, *21*, 5004-5006.

(3) Stankovich, S.; Dikin, D. A.; Piner, R. D.; Kohlhaas, K. A.; Kleinhammes, A.; Jia, Y. Y.; Wu, Y.; Nguyen, S. T.; Ruoff, R. S. *Carbon* **2007**, *45*, 1558-1565.

(4) Szabó, T.; Tombácz, E.; Illés, E.; Dékány, I. *Carbon* **2006**, *44*, 537-545.

(5) Shen, J. F.; Yan, B.; Shi, M.; Ma, H. W.; Li, N.; Ye, M. X. *J. Mater. Chem*. **2011**, *21*, 3415-3421.

(6) Xiang, Q. J.; Yu, J. G.; Jaroniec, M. *J. Phys. Chem. C* **2011**, *115*, 7355-7363.

(7) Bao, N. Z.; Shen, L. M.; Takata, T.; Domen, K. *Chem. Mater*. **2008**, *20*, 110-117.